MACE-PINNs: Multi-Network Driven Decoupling of Interdependent Physics in Coupled PDE Systems

by

Rushir Manojkumar Bhavsar

A Thesis
Presented in Partial Fulfillment
of the Requirements for the Degree
Master of Science

Approved April 2025 by the
Graduate Supervisory Committee

Kookjin Lee, Chair
Hokeun Kim
Yanjie Fu
Yoojung Choi

ARIZONA STATE UNIVERSITY
May 2025

ABSTRACT

Physics-Informed Neural Networks (PINNs) provide an innovative framework for solving complex nonlinear Partial Differential Equations (PDEs) by embedding the governing equations directly into neural networks. Recent advancements have sought to improve their performance, yet standard ("vanilla") PINNs frequently encounter instabilities and inaccuracies, particularly for PDEs with coupled variables or dynamic constraints. These limitations stem from stiff gradient dynamics and multi-scale nonlinear interactions. Traditional strategies, such as time marching and curriculum training, have been employed to mitigate these issues but often yield error magnitudes higher than anticipated, reducing their effectiveness for certain PDE classes. To address these challenges, the Multi-network Architecture for Coupled Equations Physics-Informed Neural Networks (MACE-PINNs) is introduced. This approach employs parallel subnetworks to independently approximate coupled variables, interconnected via iterative residual constraints. Inspired by classical numerical solvers, this decoupled training enhances stability and learning efficiency, particularly for PDEs with sensitive initial conditions and strong parameter dependencies. MACE-PINNs is evaluated on the Gray-Scott-2D reaction-diffusion system (RDS) and the Ginzburg-Landau-2D equation—canonical examples of spatiotemporal pattern formation and intrinsic instabilities. This method integrates Fourier feature embeddings to enhance diffusion dynamics representation and adaptive gradient-norm weighting to balance residual loss with data-driven soft temporal regularization. Experimental results demonstrate robust pattern reproduction spanning 5 parametric variations for each RDS, with L2 errors ranging from 10^{-3} to 10^{-2}. This approach, inspired by classical numerical solvers, employs structured decoupling to achieve stable and physically meaningful neural approximations of complex PDE systems.

DEDICATION

To my Mother, my Father, and my elder brother, Ruchir—this work is my heartfelt promise to you. Your love, strength, and belief in me light my way, and I dedicate this to the excellence and success we dream of together.

ACKNOWLEDGMENTS

This work is a reflection of the gratitude I hold for those who've guided me along the way. To my Mother, your endless love and gentle strength keep me steady; to my Father, your wise words and quiet support point me forward; and to my elder brother, Ruchir, your constant presence and encouragement lift me up—your trust in me shines through every step. I'm so thankful for my Thesis Chair, whose steady belief in me helped this project bloom into something real. To my committee member faculties, your incredible kindness and insight came just when I needed it most, pulling me through with quick, caring support—I'll always remember that boost. And to my friends and colleagues, your laughter, advice, and little acts of help turned tough days into bright ones. This thesis belongs to all of you, and I'm truly grateful.

TABLE OF CONTENTS

LIST OF TABLES

LIST OF FIGURES

Chapter 1

INTRODUCTION

PINNs have garnered intense interest as a flexible and data-efficient framework for leveraging deep learning in scientific and engineering problems (Raissi *et al.* (2020); Sun *et al.* (2020); Karniadakis *et al.* (2021); Raissi *et al.* (2019); Sahli Costabal *et al.* (2020)). By embedding governing equations and physical constraints directly into the loss function, PINNs promise a seamless integration of observational data and fundamental laws, thereby offering an attractive alternative to purely data-driven models when experimental or simulation data are sparse (Kissas *et al.* (2020); Fang and Zhan (2019); Liu and Wang (2019); Chen *et al.* (2020); Zhang *et al.* (2020); Haghighat and Juanes (2021); Smith *et al.* (2022)). Indeed, PINNs have been deployed successfully in a wide array of computational tasks, spanning fluid mechanics (Jin *et al.* (2020); Mathews *et al.* (2021)), bio-engineering, and meta-material design. However, practical deployments have also highlighted persistent training pathologies. These include spectral bias, by which fully connected networks struggle to represent high-frequency or multi-scale solutions (Rahaman *et al.* (2019); Cao *et al.* (2019); Tancik *et al.* (2020); Basri *et al.* (2020)), and gradient flow stiffness, wherein mismatched residual terms in the PINN loss induce gradient imbalances that hamper or even derail convergence (Zhu *et al.* (2019); Wang *et al.* (2020, 2022)).

To tackle such training obstacles, numerous strategies have been proposed. Loss re-weighting and adaptive weighting schemes dynamically reconcile the relative importance of PDE residuals and data-matching objectives (Bischof and Kraus (2021); McClenny and Braga-Neto (2020); Maddu *et al.* (2022)). Adaptive sampling of collocation points—via importance sampling, evolutionary algorithms, or residual-based

heuristics—further addresses local regions of large PDE error (Hanna *et al.* (2021); Tang *et al.* (2021); Nabian *et al.* (2021); Wu *et al.* (2023)). Meanwhile, architectural innovations like Fourier feature embeddings and positional encodings directly target spectral bias, offering improved representations of complex or oscillatory solutions (Sitzmann *et al.* (2020)). Other works explore variational and operator-based formulations, replacing pointwise PDE constraints with weak or operator-theoretic enforcement (Lagaris *et al.* (1998); Lu *et al.* (2021); Li *et al.* (2020); Kharazmi *et al.* (2021); Patel *et al.* (2022)), or coupling numerical differentiation with deep learning (Huang and Alkhalifah (2024)) to ameliorate ill-conditioning. Despite these advances, training can remain fragile for multi-physics systems with strong nonlinearities or stiff dynamics Krishnapriyan *et al.* (2021).

Traditional solver methods, like finite elements, differences, and volumes, have been the foundation of large-scale PDE simulations in engineering and applied sciences. Extensive research spanning several decades has refined these methods, establishing rigorous discretization and linearization procedures to ensure numerical stability, accompanied by thorough analyses of error bounds and convergence properties (Zienkiewicz *et al.* (2005); LeVeque (2007, 2002); Brenner and Scott (2008); Strikwerda (2004)). However, despite their maturity and robustness, these numerical techniques can still encounter instability issues when dealing with PDEs characterized by significant nonlinearities or extreme sensitivity to initial and boundary conditions. Such equations may inherently exhibit chaotic or rapidly diverging behaviors, where minor perturbations lead to trivialized, oscillatory, or blow-up solutions even at the continuous level (Quittner and Souplet (2007); Hyman and Nicolaenko (1986)). This emphasizes the ongoing difficulty of handling numerical instabilities in PDEs, highlighting the need for adaptable computational strategies that accommodate, rather than suppress, these inherent instabilities.

Such an iterative decoupling approach—employing solver-like residual checks separate from the standard physics-informed neural network (PINN) training loop—can offer fresh insights into multilayer perceptron (MLP)-based methods by addressing intrinsic stability issues. Specifically, by iteratively and independently training networks corresponding to different coupled variables, complemented by PDE-informed residual assessments, this methodology effectively blends the flexibility inherent to deep-learning architectures with stability concepts traditionally associated with classical numerical solvers. Consequently, MLPs can better adaptively capture complex solution manifolds, especially when confronted with strongly coupled or multi-scale phenomena.

To systematically explore how this strategy enhances MLP performance, we consider nonlinear PDE systems notorious for exhibiting spatiotemporal instabilities, scenarios typically challenging for standard PINN implementations. The Gray–Scott reaction–diffusion model, for example, exhibits a diverse spectrum of dynamically evolving pattern structures that are highly sensitive to slight parameter shifts and initial conditions, rendering it a valuable benchmark for testing adaptive sampling and constraint-decoupling techniques. Likewise, the Ginzburg–Landau equation, widely studied for modeling intricate wave dynamics and phase transitions prevalent in superconductivity and pattern formation Geneva and Zabaras (2020); Darbon *et al.* (2020), provides a demanding scenario to evaluate robustness against multi-scale behaviors. We develop and benchmark a parallel iterative learning architecture, which updates multiple coupled networks sequentially in parallel. Although similar in concept to adversarial training, our approach specifically targets enforcing PDE constraints. Our goal is to test whether multilayer perceptron (MLP)-based models can effectively learn underlying physics, maintaining stability even in highly nonlinear situations or when data is sparse.

The primary focus of this thesis is to enhance PINN performance through parallel subnetworking and adaptive training methods within a physics-informed framework. The main contributions are:

1. We introduce a PINN architecture featuring parallel subnetworks to independently predict the coupled variables u and v of the Gray-Scott system. This design, inspired by iterative solver decoupling and Fourier feature embeddings, improves the network's ability to capture distinct dynamics efficiently.

2. We implement a gradient norm-based adaptive loss weighting strategy that dynamically adjusts the influence of initial condition, data, and residual loss terms during training. This approach mitigates optimization challenges in coupled PDEs, outperforming standard multilayer perceptron (MLP) baselines.

3. We conduct a comprehensive sensitivity analysis of the approach for Reaction-Diffusion models such Gray-Scott model and Ginzburg-Landau model across multiple parameter variations, using five distinct datasets each. This study also evaluates the proposed parallel subnetwork PINN against a traditional MLP, demonstrating superior handling of initial condition perturbations and reaction-diffusion parameters.

Chapter 2

BACKGROUND

Physics-Informed Neural Networks

Following the benchmark framework of Scientific Machine Learning introduced in Raissi *et al.* (2019); Karniadakis *et al.* (2021), PINNs are deep learning models designed to approximate PDE solutions by embedding physical constraints directly into network training. Unlike purely data-driven methods, PINNs incorporate PDEs, initial, and boundary conditions as penalty terms within a unified optimization, enabling neural networks to produce physically consistent predictions that generalize beyond limited observational data.

Mathematical Formulation

Consider a general PDE defined on a spatiotemporal domain $[0, T] \times \Omega$, with $\Omega \subset \mathbb{R}^d$ a bounded spatial region:

$$\frac{\partial u}{\partial t}(t, \mathbf{x}) + \mathcal{D}[u](t, \mathbf{x}) = f(t, \mathbf{x}), \quad (t, \mathbf{x}) \in [0, T] \times \Omega, \tag{2.1}$$

where $\mathcal{D}[\cdot]$ denotes a differential operator, possibly nonlinear, and $u(t, \mathbf{x})$ is the unknown solution. The PDE is complemented by an initial condition

$$u(0, \mathbf{x}) = g(\mathbf{x}), \quad \mathbf{x} \in \Omega, \tag{2.2}$$

and boundary conditions represented in a general abstract form as:

$$\mathcal{B}[u](t, \mathbf{x}) = h(t, \mathbf{x}), \quad (t, \mathbf{x}) \in [0, T] \times \partial\Omega, \tag{2.3}$$

where the boundary operator $\mathcal{B}[\cdot]$ can encode Dirichlet, Neumann, Robin, or periodic conditions.

Neural Network Approximation and PDE Residual

In PINNs, the solution $u(t, \mathbf{x})$ of the PDE is approximated by a neural network $u_\theta(t, \mathbf{x})$, parameterized by weights and biases collected in θ. Activation functions like hyperbolic tangent (tanh) or swish facilitate efficient computation of second-order derivatives via automatic differentiation, crucial for accurate PDE residual evaluations. To enforce adherence to PDE constraints throughout the entire computational domain, including the domain interior, initial conditions, and boundary conditions, we define a unified residual term as follows:

$$\mathcal{R}[u_\theta](t, \mathbf{x}) = \begin{cases} \frac{\partial u_\theta}{\partial t}(t, \mathbf{x}) + \mathcal{D}[u_\theta](t, \mathbf{x}) - f(t, \mathbf{x}), & (t, \mathbf{x}) \in [0, T] \times \Omega, \quad \textit{(Interior)} \\ u_\theta(0, \mathbf{x}) - g(\mathbf{x}), & (t, \mathbf{x}) \in \{0\} \times \Omega, \quad \textit{(Initial)} \\ \mathcal{B}[u_\theta](t, \mathbf{x}) - h(t, \mathbf{x}), & (t, \mathbf{x}) \in [0, T] \times \partial\Omega, \quad \textit{(Boundary)} \\ u_\theta(t, \mathbf{x}) - \hat{u}(t, \mathbf{x}), & (t, \mathbf{x}) \in \mathcal{D}_{\text{data}}, \quad \textit{(Data)} \end{cases} \tag{2.4}$$

where $\mathcal{D}_{\text{data}}$ represents the subset of the domain at which observational or simulated data $\hat{u}(t, \mathbf{x})$ are available.To evaluate this residual term, *collocation points* are sampled across the domain's interior, boundaries, and initial conditions, serving as locations for explicit enforcement of PDE residuals. The neural network parameters θ are optimized by minimizing the composite loss defined over a suitable set of collocation points $\{(t_i, \mathbf{x}_i)\}_{i=1}^N$ sampled across the complete domain and boundary:

$$\mathcal{L}(\theta) = \frac{1}{N} \sum_{i=1}^{N} \|\mathcal{R}[u_\theta](t_i, \mathbf{x}_i)\|^2. \tag{2.5}$$

Optimization is typically performed using gradient-based algorithms such as stochastic gradient descent or Adam, ensuring that the trained neural network closely satisfies the governing physics across the entire computational domain.

Case Study: The Gray-Scott Equation

The Gray-Scott model is a canonical reaction–diffusion system characterized by its ability to generate rich and diverse spatial-temporal patterns. This system describes the interaction and diffusion of two chemical species, $u(t, \mathbf{x})$ and $v(t, \mathbf{x})$, defined over a two-dimensional periodic domain $\Omega = [0, 2\pi]^2$:

$$\frac{\partial u}{\partial t} = D_u \Delta u - uv^2 + F(1 - u), \tag{2.6}$$

$$\frac{\partial v}{\partial t} = D_v \Delta v + uv^2 - (F + k)v, \tag{2.7}$$

where $u(t, \mathbf{x})$ and $v(t, \mathbf{x})$ represent the concentrations of chemical species, $D_u, D_v > 0$ are their respective diffusion coefficients, and Δ denotes the two-dimensional Laplacian operator given by

$$\Delta = \frac{\partial^2}{\partial x^2} + \frac{\partial^2}{\partial y^2}$$

The model is defined on a periodic spatial domain $\Omega = [0, 2\pi]^2$, satisfying boundary conditions:

$$u(t, x, y)\big|_{x=0} = u(t, x, y)\big|_{x=2\pi}, \quad v(t, x, y)\big|_{x=0} = v(t, x, y)\big|_{x=2\pi},$$

and analogously for the y-coordinate, with initial conditions given by

$$u(0, \mathbf{x}) = u_0(\mathbf{x}) \tag{2.8}$$

$$v(0, \mathbf{x}) = v_0(\mathbf{x}) \tag{2.9}$$

Dynamics, Stability, and Pattern Formation

The Gray-Scott equations model autocatalytic chemical reactions coupled with diffusion, exhibiting classical Turing-type instabilities. Under certain parameter conditions, a uniform equilibrium can spontaneously destabilize, leading to the formation of diverse spatial-temporal patterns such as spots, stripes, or chaotic structures. The

system's dynamics depend sensitively on the diffusion coefficients (D_u, D_v) and reaction parameters (F, k). Small variations in these parameters significantly influence stability thresholds and the complexity of emergent patterns. Table 2.1 summarizes these key parameters, outlining their physical meanings and their impact on pattern formation dynamics.

Table 2.1: Key Parameters of the Gray-Scott Reaction–Diffusion Model.

Parameter	**Physical Interpretation**	**Influence on Dynamics and Stability**
D_u	Diffusion of activator (u)	Controls spatial scale, direct proportionality
D_v	Diffusion of inhibitor (v)	Modulates sharp pattern complexity.
F	Feed rate (chemical input)	Induces oscillations or chaos.
k	Reaction (removal) rate	Triggers pattern transitions.

Significance and Application

The Gray-Scott model is a fundamental example of reaction–diffusion systems widely employed to investigate pattern-forming mechanisms in chemistry, biology, and materials science. Practically, it models chemical reactions exhibiting spontaneous pattern formation, such as autocatalytic processes seen in laboratory chemical oscillators. In biology, it captures essential aspects of developmental processes, including skin pigmentation patterns and morphogenetic signals responsible for biological pattern formation. The model's sensitivity to parameters has made it an effective benchmark for evaluating the performance and stability of numerical solvers, particularly when handling stiff equations and multi-scale dynamics characteristic of reaction–diffusion systems.

Case Study: Ginzburg–Landau Equation

The complex Ginzburg–Landau equation provides a canonical example of nonlinear PDEs describing pattern formation and amplitude dynamics in various physical systems, including superconductivity, superfluidity, and nonlinear optics. We consider the complex scalar field $A(\mathbf{x}, t)$ governed by the following PDE over a two-dimensional spatial domain $\Omega = [-1, 1]^2$ with periodic boundary conditions:

$$\frac{\partial A}{\partial t} = \epsilon \Delta A + \mu A - \gamma |A|^2 A, \tag{2.10}$$

where $A(\mathbf{x}, t) \in \mathbb{C}$, Δ denotes the 2D Laplacian, and parameters ϵ, $\mu \in \mathbb{R}$ and $\gamma \in \mathbb{C}$ control the diffusive, linear, and nonlinear behaviors, respectively.

By decomposing $A = u + iv$ into real (u) and imaginary (v) parts, the equation separates into the following coupled real-valued PDE system:

$$\frac{\partial u}{\partial t} = \epsilon \Delta u + \mu u - \mathrm{Re}(\gamma)(u^2 + v^2)u + \mathrm{Im}(\gamma)(u^2 + v^2)v, \tag{2.11}$$

$$\frac{\partial v}{\partial t} = \epsilon \Delta v + \mu v - \mathrm{Re}(\gamma)(u^2 + v^2)v - \mathrm{Im}(\gamma)(u^2 + v^2)u, \tag{2.12}$$

where $\mathrm{Re}(\gamma)$ and $\mathrm{Im}(\gamma)$ are the real and imaginary parts of γ.

Stability, Dynamics, and Pattern Formation

Solutions of the Ginzburg–Landau equation exhibit rich dynamical regimes ranging from stable uniform states and traveling waves to complex vortex patterns and amplitude chaos, strongly influenced by parameters ϵ, μ, and γ. These dynamics are sensitive to parameter variations, often transitioning abruptly between stable and chaotic regimes. Notably, subtle changes in the imaginary part of the nonlinear parameter γ can induce transitions from stable spiral wave patterns to turbulent or chaotic dynamics, highlighting the system's rich bifurcation structure. The periodic

boundary conditions further complicate these dynamics by permitting wave interactions across domain boundaries, effectively enabling long-range spatial coupling. Such sensitivity to parameter and boundary conditions poses significant numerical challenges, making accurate solution methods particularly valuable for investigating complex wave phenomena. Table 2.2 summarizes these parameters and their significance.

Table 2.2: Key Parameters of the Complex Ginzburg–Landau Equation.

Parameter	**Physical Interpretation**	**Influence on Dynamics and Stability**
ϵ	Diffusion strength	Affects spatial smoothness and solution scale
μ	Linear growth rate	Controls growth or decay of wave amplitude
$\mathrm{Re}(\gamma)$	Nonlinear saturation	Amplitude saturation and pattern regulation
$\mathrm{Im}(\gamma)$	Nonlinear dispersion	Complex oscillations and wave modulation.

Significance and Application

The Ginzburg–Landau equation serves as a foundational model for a variety of practical phenomena across scientific and engineering disciplines. It describes vortex lattices and filamentary structures in superconductors, spiral and scroll waves in chemical reactions such as the Belousov–Zhabotinsky reaction, and amplitude modulation in nonlinear optics, particularly in fiber lasers and optical cavities. In fluid dynamics, it models the amplitude and phase behavior of near-critical Rayleigh–Bénard convection patterns. As a prototypical equation governing nonlinear wave interactions, it provides critical insights into the control and prediction of instabilities in engineering applications, ranging from the suppression of turbulence in fluid flows to the design of stable modes in optical waveguides.

Comparitive Remarks

The Gray–Scott and Ginzburg–Landau equations exemplify nonlinear PDE systems characterized by distinct yet related pattern-forming instabilities. The former captures chemical reaction–diffusion dynamics leading to localized activator-inhibitor patterns, while the latter describes complex amplitude-phase modulations often manifesting as vortices or spiral waves. Both systems feature PDE residuals with nonlinear polynomial interactions that complicate numerical solution landscapes.

To efficiently resolve these nonlinearities and capture multi-scale periodic solutions, appropriate augmentation of neural network input features is essential. Techniques such as Fourier feature embeddings (FFEs) or spectral transformations can enhance a neural solver's ability to learn intricate periodic patterns and nonlinear residual terms. This is reflected in key aspects—nonlinearities, pattern types, residual complexity, and potential feature augmentations—summarized in Table 2.3, which provides a concise comparison to guide our implementation strategies.

Table 2.3: Comparison of Nonlinearities, Patterns, Residuals, and Feature Augmentations.

Aspect	**Gray–Scott Model**	**Ginzburg–Landau Model**
Dominant Nonlinearity	Cubic polynomial (uv^2)	Cubic polynomial ($\|A\|^2A$)
Solution Patterns	Spots, stripes	Spirals, vortices
Residual Complexity	Coupled polynomial reactions	Complex polynomial amplitude interactions
Suitable Feature Augmentation	Spectral/Fourier features	Fourier/sinusoidal embedding

Chapter 3

METHODOLOGY

Outline

This chapter details our methodological approach for solving complex coupled PDE systems using our novel *Multi-network Architecture for Coupled Equations Physics-Informed Neural Networks* (**MACE-PINNs**). Our experiments target two challenging systems—the ***Gray–Scott*** reaction–diffusion model and the ***Ginzburg–Landau*** equation—which are characterized by intricate nonlinear dynamics and fine-scale spatial patterns. The following sections elaborate on the architecture design, training strategy, loss formulation, and input feature augmentation techniques that form the foundation of our approach.

Architecture Design

Figure 3.1 provides a conceptual overview of the trainable block of the proposed MACE-PINNs architecture for modeling RDS. The design initiates with spatial coordinates defining the domain, which are transformed using a FFE layer to enhance the representation of high-frequency spatial patterns. Periodic boundary conditions are subsequently enforced to preserve the physical realism at the domain boundaries.

Following these preprocessing steps, the architecture employs a parallel subnetwork structure where one branch approximates the activator $u(\mathbf{x}, t)$ and the other targets the inhibitor $v(\mathbf{x}, t)$. Each branch extracts deep features through the network, effectively capturing the complex and nonlinear dynamics variable specific.

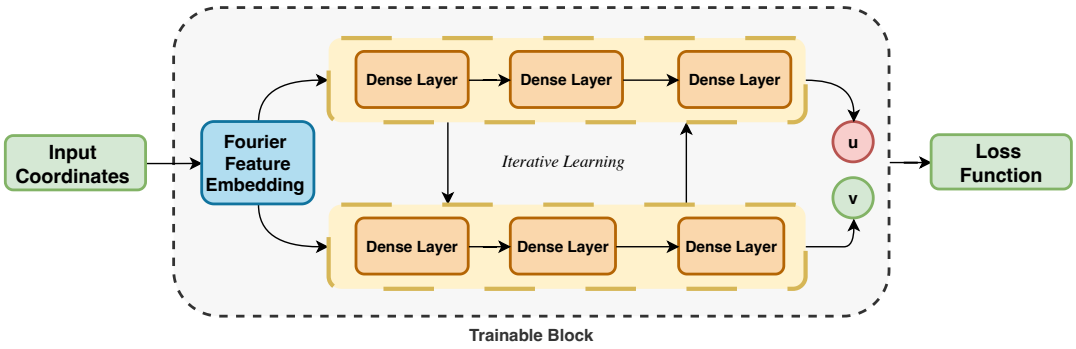

Figure 3.1: Architecture Design

The training process integrates the outputs using a training and adaptive weighing algorithm, which is coupled with a composited loss function. This iterative refinement mechanism not only enforces the physical coupling prescribed by the governing PDEs but also progressively enhances the predictive accuracy of the model.

Input Preprocessing and Architectural Enhancements

Periodic Boundary Enforcement The Gray–Scott and Ginzburg–Landau systems evolve on a periodic domain $\Omega = [-1, 1]^2$, requiring strict adherence to $u(x, y, t) = u(x + 2, y, t)$ and $v(x, y, t) = v(x + 2, y, t)$. We hardwire periodicity into the architecture through a coordinate transformation:

$$(x', y') = (\text{mod}(x + 1, 2) - 1,\ \text{mod}(y + 1, 2) - 1)\,, \tag{3.1}$$

where mod denotes the modulo operation. This guarantees $u(x', y', t) \equiv u(x, y, t)$ by design, eliminating boundary mismatch errors.

Fourier Feature Embedding To overcome neural networks' spectral bias and capture high-frequency patterns in reaction–diffusion systems, we preprocess inputs

$\mathbf{z} = (x', y', t)$ using random Fourier features (RFF):

$$E(\mathbf{z}) = \left[\sin(B\mathbf{z}), \cos(B\mathbf{z})\right]^\top \in \mathbb{R}^P, \tag{3.2}$$

with parameters:

- $B \in \mathbb{R}^{(P/2)\times 3} \sim \mathcal{N}(0, \sigma^2)$: Random frequency matrix
- $P = 128$: Embedding dimension
- $\sigma = 6$: Learnable frequency scaling parameter

This RFF projection, applied to the periodic coordinates (x', y'), enables simultaneous resolution of:

- High-frequency spatial patterns through Fourier basis components
- Long-range temporal correlations via direct time coordinate processing

The combined preprocessing pipeline first enforces periodicity then enriches spectral representation, as theoretically justified by Fourier-augmented networks' capacity to learn multiscale features Tancik *et al.* (2020).

Subnetwork Structure

The MACE-PINNs architecture employs two subnetworks (MLPs) to independently approximate the system variables u and v:

$$u_\theta(\mathbf{x}) = \mathrm{MLP}_\theta(E(\mathbf{x})), \quad v_\phi(\mathbf{x}) = \mathrm{MLP}_\phi(E(\mathbf{x})), \tag{3.3}$$

with the shared Fourier-embedded input $E(\mathbf{x}) \in \mathbb{R}^{128}$. Each subnetwork consists of three hidden layers:

$$E(\mathbf{x}) \in \mathbb{R}^{128} \xrightarrow[\tanh]{H_1=64} \mathbb{R}^{64} \xrightarrow[\text{swish}]{H_2=64} \mathbb{R}^{64} \xrightarrow[\tanh]{H_3=32} \mathbb{R}^{32} \to \mathbb{R}.$$

Weights are initialized with He-normal initialization, and biases are zero-initialized. The decoupled design mitigates gradient conflicts, and physical coupling between u and v is explicitly enforced via the PDE residual loss.

Composite Loss Function with Adaptive Weighting

Building on the unified PINNs framework (Eqs.(2.1)–(2.5)), the training of MACE-PINNs integrates physical consistency through a weighted combination of three loss components, dynamically balanced via gradient-based adaptation:

- **Initial Condition Loss** (for variables $k \in \{u, v\}$): Enforces alignment with prescribed initial states using $N_{\text{ic}} = 40{,}000$ samples:

$$\mathcal{L}_{\text{ic}_k} = \frac{1}{N_{\text{ic}}} \sum_{i=1}^{N_{\text{ic}}} \left(k_\theta(\mathbf{x}_i, 0) - k_0(\mathbf{x}_i)\right)^2$$

- **Data Loss**: Regularizes predictions against N_d spatio-temporal reference snapshots:

$$\mathcal{L}_{\text{data}_k} = \frac{1}{N_d} \sum_{j=1}^{N_d} \left(k_\theta(\mathbf{x}_j, t_j) - k_{\text{ref}}(\mathbf{x}_j, t_j)\right)^2$$

- **PDE Residual Loss**: Encodes reaction–diffusion dynamics via residuals $r_k(\mathbf{x}, t)$ evaluated at $N_r = 4096 \times 64$ collocation points:

$$\mathcal{L}_{\text{res}_k} = \frac{1}{N_r} \sum_{l=1}^{N_r} \left(r_k(\mathbf{x}_l, t_l)\right)^2$$

The total loss combines these terms with adaptively tuned weights $\lambda_i^{(t)}$:

$$\mathcal{L}_{\text{total}} = \sum_{k \in \{u,v\}} \left(\lambda_{\text{ic}_k}^{(t)} \mathcal{L}_{\text{ic}_k} + \lambda_{\text{data}_k}^{(t)} \mathcal{L}_{\text{data}_k} + \lambda_{\text{res}_k}^{(t)} \mathcal{L}_{\text{res}_k} \right), \qquad \lambda_i^{(t)} = \frac{\|\nabla_\theta \mathcal{L}_i^{(t)}\|}{\sum_j \|\nabla_\theta \mathcal{L}_j^{(t)}\|}. \quad (3.4)$$

where weights are updated at training epoch t using gradient norm ratios, i.e., by computing the norm of the gradient of each loss component with respect to the network parameters. To ensure stability, weights are smoothed via exponential averaging:

$$\hat{w}_i^{(t)} = \alpha \hat{w}_i^{(t-1)} + (1 - \alpha) w_i^{(t)}, \quad \alpha \in (0, 1), \tag{3.5}$$

with initial condition $\hat{w}_i^{(0)} = w_i^{(0)}$. This adaptively prioritizes loss components based on their gradient influence while mitigating abrupt training fluctuations.

Iterative Training and Adaptive Weighing Algorithm

Algorithm 1 MACE-PINNs Iterative Training with Adaptive Weighting

Input: $\mathcal{C}$ (epochs, lr, wu_freq, etc.), $\mathcal{D}$, $\Lambda = \{\lambda^u_{\text{ic}}, \lambda^u_{\text{data}}, \lambda^u_{\text{res}}, \lambda^v_{\text{ic}}, \lambda^v_{\text{data}}, \lambda^v_{\text{res}}\}$
Output: $\mathcal{S}$
RNG $\leftarrow$ `PRNGKey`($\mathcal{C}_{\text{seed}}$), $\mathcal{S} \leftarrow$ `InitTrainState`(RNG, $\mathcal{C}$, $\mathcal{D}$), $\alpha \leftarrow 0.9$
$\mathcal{B} \leftarrow$ `GatherWindowData`($\mathcal{D}$, 0, $\mathcal{C}_{\text{min\_window\_size}}$)
for epoch $= 1$ to $\mathcal{C}_{\text{epochs}}$ **do**
    Adjust t_{end} via $\{(0.2 \cdot \mathcal{C}_{\text{epochs}}, 20), \ldots, (1.0 \cdot \mathcal{C}_{\text{epochs}}, 100)\}$
    if stage update **then**
        $\mathcal{B} \leftarrow$ `GatherWindowData`($\mathcal{D}$, 0, t_{end})
    end if
    $\mathcal{P} \leftarrow$ `SampleCollocationPoints`($\mathcal{D}_{\text{x}}$, $\mathcal{D}_{\text{y}}$, $\mathcal{D}_{\text{t}}[0 : t_{\text{end}}]$)
    for $n \in \{u, v\}$ **do**
        $\theta_{\text{other}} \leftarrow$ `Freeze`($\mathcal{S}.\theta_{\text{other}}$), $\mathcal{K} \leftarrow$ `Freeze`($\{\epsilon_1, \epsilon_2, b_1, b_2, c_1, c_2\} \cup \Lambda_n$)
        $(\mathcal{S}, M_n) \leftarrow$ `Backprop`($\mathcal{S}$, $L_n(\mathcal{B}, \mathcal{P}, \mathcal{K})$, update θ_n)
    end for
    if epoch $\mod \mathcal{C}_{\text{wu\_freq}} = 0$ **and** epoch > 0 **then**
        $G \leftarrow$ `ComputeGradNorms`($\mathcal{S}$, $\mathcal{B}$, $\mathcal{P}$, $\mathcal{K}$), $G^{u/v}_{\text{total}} \leftarrow \sum_{c \in \{\text{ic,data,res}\}} G^{u/v}_c$
        for $c \in \{\text{ic}, \text{data}, \text{res}\}$ **do**
            $\lambda^{u/v}_c \leftarrow \alpha \cdot \lambda^{u/v}_c + (1 - \alpha) \cdot (G^{u/v}_{\text{total}} / (G^{u/v}_c + 10^{-8}))$
        end for
        $\Lambda^{u/v} \leftarrow$ `clip`($\Lambda^{u/v} / \sum \Lambda^{u/v}$, 0.01, 1.0)
    end if
end for
return `SaveCheckpoint`($\mathcal{S}$, $\mathcal{C}_{\text{epochs}}$)

The subnetworks $u_\theta(\mathbf{x})$ and $v_\phi(\mathbf{x})$ are trained in an epoch-wise alternating schedule, where we freeze v_ϕ and update u_θ to minimize its residual, data, and boundary losses. At epoch $k+1$ the roles reverse, isolating the gradient flow of v_ϕ. This single-epoch cadence suppresses inter-variable interference and smooths the loss landscape. This strict separation eliminates inter-variable gradient interference and smooths the loss landscape.Using one optimizer preserves memory efficiency and streamlines hyper-parameter tuning. The strategy extends naturally to more coupled fields by rotating the active parameter set each epoch.

Chapter 4

THEORETICAL CONSIDERATIONS

This chapter presents a theoretical investigation into the limitations faced by Physics-Informed Neural Networks (PINNs) in modeling nonlinear reaction–diffusion systems, with a focus on the Gray–Scott and Ginzburg–Landau equations. These systems exhibit complex dynamics characterized by strong spatial coupling, multi-scale interactions, and pronounced sensitivity to parameter variations. We identify two core challenges that hinder accurate PINN approximation: (i) the instability introduced by second-order spatial derivatives in the Laplacian operator, and (ii) parametric sensitivity leading to abrupt dynamical transitions. By formalizing these issues through linear stability analysis and examining their implications for training dynamics, we motivate the architectural and algorithmic enhancements introduced in later chapters.

Reaction-Diffusion Systems and the Laplacian Operator

Reaction-diffusion systems describe spatial-temporal processes governed by both nonlinear reaction terms and spatial diffusion. Such systems commonly arise in chemical, physical, and biological contexts and are mathematically expressed through PDEs incorporating the Laplacian operator (∇^2). A generic form of reaction-diffusion equations can be represented as:

$$\frac{\partial u}{\partial t} = D\nabla^2 u + R(u), \tag{4.1}$$

where D denotes the diffusion coefficient, and $R(u)$ encapsulates the nonlinear reaction dynamics.

The Laplacian operator is central to these equations, governing how spatial variations propagate and dissipate. Accurate representation of this term is critical for numerical methods, including PINNs. However, the Laplacian introduces notable computational challenges—particularly for spatially sparse data or sharply varying solutions—due to its second-order spatial derivatives.

Laplacian Stability Analysis

To better understand Laplacian-induced instability, we consider the linearized dynamics near a spatially uniform equilibrium u_0 such that $R(u_0) = 0$. Introducing a small perturbation δu, we obtain the linearized PDE:

$$\frac{\partial \delta u}{\partial t} = D\nabla^2 \delta u + R'(u_0)\delta u. \tag{4.2}$$

Assuming a Fourier mode decomposition $\delta u \sim e^{i\mathbf{k}\cdot\mathbf{x}+\lambda t}$, the resulting dispersion relation becomes:

$$\lambda(\mathbf{k}) = -D|\mathbf{k}|^2 + R'(u_0). \tag{4.3}$$

The system becomes unstable when $\lambda(\mathbf{k}) > 0$, i.e., when $R'(u_0) > D|\mathbf{k}|^2$. This condition defines a threshold below which long-wavelength perturbations ($|\mathbf{k}|$ small) grow in time, triggering pattern formation or oscillatory instabilities. For numerical solvers, including PINNs, this necessitates precise estimation of second-order derivatives to avoid artificially damping or amplifying such modes.

Challenges for PINNs: Accurate Laplacian Approximation

While automatic differentiation allows PINNs to compute spatial derivatives without explicit discretization, this approach introduces numerical instability when approximating second-order derivatives—such as the Laplacian—especially in regimes with sharp gradients or high-frequency features. Neural networks, particularly multi-

layer perceptrons (MLPs), exhibit spectral bias, favoring low-frequency solutions and thereby underrepresenting the oscillatory components critical for accurate Laplacian reconstruction Rahaman *et al.* (2019); Tancik *et al.* (2020).

As a result, training often stagnates or diverges due to noisy residuals or imbalanced gradient magnitudes across the domain. These inaccuracies are particularly detrimental when approximating PDEs prone to instability, where even small errors in the Laplacian can amplify dramatically.

Parametric Sensitivity in Reaction-Diffusion Systems

This sensitivity can be characterized by bifurcation theory, where the system transitions from stable equilibria to pattern-forming or chaotic regimes as parameters cross critical thresholds. For example, in the Gray–Scott system, the onset of Turing instability is governed by the ratio of diffusion coefficients and reaction terms. An illustrative bifurcation condition for activator–inhibitor systems is: $F \cdot k < D_u \cdot D_v$ (Turing instability condition) which marks the transition from homogeneous to patterned solutions. In such settings, even minor parameter shifts ($\Delta F \sim 10^{-3}$) can drastically alter qualitative behavior, requiring PINNs to generalize across a high-dimensional, discontinuous solution manifold. Without tailored architectural support, neural networks risk overfitting to specific parametric configurations and fail to capture such transitions.

Such parametric sensitivity poses substantial demands on PINNs: networks must robustly generalize across vast, diverse solution spaces, handling nonlinear transitions and instabilities arising from minute parameter perturbations. PINNs trained inadequately—either due to insufficient parameter sampling, lack of robust regularization, or restricted network capacity—risk overfitting to limited regimes, thereby limiting generalization.

Specific Reaction-Diffusion Examples

We illustrate the above theoretical concerns with two canonical examples: the Gray–Scott and Ginzburg–Landau equations. The Gray–Scott model describes nonlinear chemical reactions coupled with diffusion:

$$\frac{\partial u}{\partial t} = D_u \nabla^2 u - uv^2 + F(1-u), \quad (4.4) \qquad \frac{\partial v}{\partial t} = D_v \nabla^2 v + uv^2 - (F+k)v. \quad (4.5)$$

Its stability depends intricately upon diffusion coefficients (D_u, D_v), the feed rate F, and kill rate k. The interplay between diffusion and nonlinear reaction terms dictates the emergence of spatial patterns or instabilities.

Similarly, the complex-valued Ginzburg–Landau equation:

$$\frac{\partial A}{\partial t} = A - (1+i\beta)|A|^2 A + (1+i\alpha)\nabla^2 A, \quad (4.6)$$

features rich dynamics influenced by parameters α and β. The complex Laplacian term $(1+i\alpha)\nabla^2 A$ interacts with nonlinear reaction terms, enabling oscillatory instabilities, traveling waves, or chaotic dynamics under certain parameter regimes.

Interactions between Laplacian Instability and Parametric Sensitivity

The challenges of accurate Laplacian representation and parametric sensitivity are mutually reinforcing. Instabilities inherent to the PDEs magnify approximation errors in spatial derivatives computed by PINNs, further exacerbating numerical instabilities. Conversely, parameter-induced solution variability requires PINNs to accurately approximate solutions across widely divergent spatial-temporal dynamics, thereby intensifying demands on spatial derivative accuracy.

Concluding Remarks

In conclusion, PINNs face significant theoretical and practical challenges in approximating nonlinear reaction–diffusion systems. Accurately representing the Laplacian operator, especially for complex spatial variations, remains problematic due to inherent network limitations and the instability of PDE solutions. Moreover, extreme parametric sensitivity compounds these difficulties, demanding networks robust enough to generalize across highly nonlinear and diverse dynamical regimes.

These compounded challenges underscore the necessity of architectural innovations tailored to address the dual difficulties of spectral instability and parametric nonlinearity. Specifically, enhancements such as Fourier feature embeddings provide a principled mechanism to improve spectral expressivity, thereby mitigating errors in Laplacian approximation. Simultaneously, the proposed modular framework MACE-PINNs enables the decoupling of interdependent variables through parallel subnetworks, directly addressing the gradient pathologies induced by coupled dynamics. These theoretical insights motivate the architectural design presented in Chapter **??**, where both spectral and structural augmentations are integrated to stabilize training and enhance generalization across sensitive parametric regimes.

Chapter 5

EXPERIMENTS AND RESULTS

Introduction

This chapter evaluates the performance of MACe-PINNs on two canonical RDS: the Gray-Scott model and the Complex Ginzburg-Landau equation. We analyze ten simulation variations (five per system) to quantify how neural networks approximate pattern formation dynamics under varying initial conditions, parameter regimes, and boundary constraints. Results are reported using normalized L^2 errors, maximum absolute errors (MAE), and PDE residual losses.

Experimental Setup

Domain and Parameters: Both systems were simulated on the periodic domain $\Omega = [-1, 1]^2$ with identical spatial discretization (200×200 grid) and temporal resolution ($\Delta t = 0.01$). The Gray-Scott system used fixed diffusion coefficients $\epsilon_1 = 200$, $\epsilon_2 = 100$ ($k = 1000$), while the Ginzburg-Landau equation employed $\epsilon = 0.004$, $\alpha = 1.5$, with $k = 10$ (except Variation GL3).

Metrics: Solution accuracy was quantified using:

- Relative L^2 error: $\|u_{\text{pred}} - u_{\text{ref}}\|_2 / \|u_{\text{ref}}\|_2$
- Maximum absolute error (MAE): $\max |u_{\text{pred}} - u_{\text{ref}}|$
- PDE residual: $\mathcal{L}_{\text{res}} = \frac{1}{N_r} \sum_{i=1}^{N_r} |r(u_i)|^2$

Simulation Variations

The Gray-Scott reaction-diffusion system exhibits a diverse range of spatiotemporal behaviors depending on the choice of reaction parameters b_1 and b_2. We explore five variations of the system, including a benchmark case (GS0) and four parameter modifications (GS1–GS4), each giving rise to distinct emergent patterns. Table 5.1 summarizes the parameter choices and their corresponding spatial patterns.

Table 5.1: Gray–Scott System Variations and Patterns

Variation	**Parameters**	**Pattern**
GS0	$b_1 = 0.04k,\ b_2 = 0.1k$	Self-replicating spots
GS1	$b_1 = 0.025k,\ b_2 = 0.085k$	Mitosis (spotted growth)
GS2	$b_1 = 0.035k,\ b_2 = 0.095k$	Striped morphology
GS3	$b_1 = 0.03k,\ b_2 = 0.09k$	Mixed spots/stripes
GS4	$b_1 = 0.0545k,\ b_2 = 0.067k$	Chaotic self-replication

Varying dynamics stem from the delicate interplay between reaction rates and diffusion processes. Self-replicating spots, as seen in *GS0*, represent a stable and periodic formation, whereas mitotic growth in *GS1* introduces a controlled expansion of patterns. In contrast, *GS2* generates striped morphologies, suggesting a shift toward anisotropic diffusion-dominated regimes. The mixed-pattern case in *GS3*, where both spots and stripes coexist, signifies an intermediate state of pattern formation with competing structural influences. Finally, *GS4*, exhibiting chaotic self-replication, represents a highly unstable regime where small perturbations can result in vastly different outcomes over time.

These variations provide a valuable framework for studying the evolution and stability of reaction-diffusion systems. Understanding how different parameter choices drive distinct pattern dynamics is essential not only for exploring the Gray-Scott

model's theoretical underpinnings but also for evaluating how well numerical approaches, such as PINNs, can capture and generalize across these regimes. Since each variation presents a unique combination of stability and complexity, analyzing them in detail allows us to assess how effectively computational methods can adapt to different diffusion-reaction conditions.

Model Results

Table 5.2: Combined Gray-Scott System Performance Metrics

Variation	Method	Residual Loss		IC Loss		Data Loss	
		U	**V**	**U**	**V**	**U**	**V**
GS0	*"vanilla" PINN*	5.28e-7	2.58e-6	1.86e-4	4.25e-3	1.77e-1	4.01e-2
	Proposed	1.64e-4	2.37e-4	2.13e-7	2.65e-7	2.68e-4	2.69e-5
GS1	*"vanilla" PINN*	1.43e-6	3.30e-6	1.61e-4	1.07e-2	7.74e-2	1.48e-2
	Proposed	1.39e-4	5.95e-4	1.46e-7	2.61e-6	1.53e-5	3.57e-5
GS2	*"vanilla" PINN*	4.33e-7	6.22e-7	1.35e-5	3.47e-3	1.31e-1	2.41e-2
	Proposed	1.41e-3	6.88e-4	4.79e-7	2.26e-7	1.69e-5	1.20e-5
GS3	*"vanilla" PINN*	7.66e-7	1.28e-6	2.20e-5	4.51e-3	1.03e-1	1.73e-2
	Proposed	1.78e-4	2.81e-4	6.07e-7	2.23e-6	1.10e-5	1.27e-5
GS4	*"vanilla" PINN*	1.30e-7	2.32e-7	1.94e-3	1.61e-3	1.31e-1	2.61e-2
	Proposed	7.12e-4	5.39e-4	2.66e-7	2.24e-6	1.87e-5	1.17e-5

For the Gray–Scott system, the proposed methodology outperforms the vanilla PINN implementation, particularly in terms of *initial condition (IC) losses* and *data losses*. Table 5.1 presents the key parameter variations which affect the complexity of training, as the network must simultaneously approximate reference data while enforcing PDE constraints under different dynamical regimes. Table 5.2 provides a detailed quantitative assessment of these performance metrics, including data, residual, and initial condition (IC) losses.

While the vanilla PINNs display IC losses often reaching 10^{-3}, the proposed method dramatically reduces these losses down to 10^{-6} and 10^{-7}. Additionally, the proposed model maintains significantly lower data losses, typically around 10^{-5}. The relationship between pattern dynamics and training performance is evident across the variations. **GS0 (Benchmark)**, which represents self-replicating spots, serves as a stable reference. The data losses are relatively small, and the residual errors are well-controlled, suggesting that PINNs effectively capture the structured, repetitive nature of the spots with minimal difficulty.

A nuanced yet essential distinction emerges in the handling of *residual losses*. Although the proposed models show numerically higher residual losses compared to their vanilla counterparts—ranging from 10^{-4} to 10^{-3} for both systems—these elevated residuals represent a conscious trade-off, facilitating more physically meaningful solutions. Conversely, deceptively low residual losses in vanilla implementations, typically on the order of 10^{-6} or 10^{-7}, mask substantial inaccuracies in data and IC conformity, implying convergence to trivial or inconsistent solutions.

GS1, characterized by mitotic (spotted growth) dynamics, introduces additional complexity in spatial pattern evolution. Here, the data loss for U is notably lower than in GS0, implying that the network efficiently fits the training data. However, the residual loss for V is significantly larger, suggesting that the evolving, non-static nature of the mitotic spots makes it more challenging for the model to enforce PDE constraints. The increase in IC loss for V further supports this observation, as the system is more sensitive to initial perturbations.

GS2, exhibiting a striped morphology, presents a dramatically different training behavior. The residual loss for U is over an order of magnitude higher than that of GS0 and GS1, despite relatively low data losses. This suggests that while the model can closely match the data, the PDE constraints are more difficult to enforce, likely

due to the sharp transitions between stripes, which create regions of high gradient variation. The IC losses remain low, indicating that initial pattern formation is well captured, but the network struggles to maintain accurate PDE representations over time.

GS3, with mixed spots and stripes, shows intermediate behavior between GS1 and GS2. The data losses are among the lowest, demonstrating strong agreement with reference solutions. However, the residual losses, particularly for U, indicate that the network faces difficulties in regions where spot-like and stripe-like structures coexist. This suggests that while PINNs are highly effective at learning either spots or stripes individually, hybrid morphologies introduce additional complexity that challenges the PDE constraint enforcement.

Finally, **GS4**, characterized by chaotic self-replication, represents the most dynamically unstable case. The data losses are still relatively low, showing that PINNs can approximate the observed patterns. However, the residual loss for U is significantly higher than all other cases except GS2, pointing to difficulties in enforcing PDE constraints in chaotic regimes. The initial condition losses for V are among the highest, reflecting the model's struggle to maintain accurate long-term predictions in a system where small perturbations can lead to drastically different outcomes.

Overall, this analysis highlights the interplay between emergent spatial patterns and training dynamics. PINNs perform exceptionally well when dealing with structured and stable morphologies, as seen in GS0 and GS1. Highly structured patterns, such as stripes (GS2), create sharp spatial variations that are difficult to resolve, while chaotic behavior (GS4) introduces sensitivity to initial conditions and long-term instabilities. These findings underscore the need for adaptive training strategies, such as loss weighting adjustments or modified network architectures, to improve performance in dynamically complex reaction-diffusion systems.

Ginzburg–Landau Reaction–Diffusion System

Simulation Variations

The Ginzburg-Landau equation describes wave phenomena (vortex nucleation, turbulence) linked to oscillatory instabilities, boundary effects, and phase turbulence. Cases GL0–GL4 (modified initial conditions) study pattern evolution—from ordered to chaotic regimes—testing computational models' ability to resolve stability, chaos, and boundary-driven dynamics.Table 5.3 summarizes the configurations and their corresponding emergent patterns.

Table 5.3: Complex Ginzburg-Landau Equation Variations and Patterns

Variation	**Initial Condition**	**Emergent Pattern**
GL0	Gaussian wave packet	*Vortex nucleation*
GL1	Multiple Gaussian bumps	*Complex patterns*
GL2	Gaussian $+ 5\cos(10x)$	*Asymmetric*
GL3	Checkerboard ($k = 5$)	*Pattern selection*
GL4	Gaussian + boundary forcing	*Turbulent*

The distinct initial conditions in all variations demonstrate the profound impact of starting configurations on the evolution and behavior of complex wave systems. From a single Gaussian wave packet in GL0 sparking vortex nucleation, to multiple bumps in GL1 forming intricate structures, an asymmetric perturbation in GL2 driving biased propagation, a checkerboard pattern in GL3 selecting dominant wavelengths, and boundary-driven perturbations in GL4 igniting turbulence. These examples collectively underscore how initial conditions serve as a critical determinant in shaping the structural and behavioral diversity of nonlinear systems, offering valuable insights into their underlying mechanics.

These variations provide a controlled setting to investigate the interplay between initial conditions and emergent complexity in the Ginzburg-Landau model. By sys-

tematically analyzing these cases, we can better understand how different perturbations influence vortex formation, pattern transitions, and turbulent states. The following sections will explore the performance of Physics-Informed Neural Networks (PINNs) in approximating these regimes, assessing their ability to learn and enforce the underlying governing equations.

Model Results

Table 5.4: Combined Ginzburg-Landau System Performance Metrics

Variation	**Method**	**Residual Loss**		**IC Loss**		**Data Loss**	
		U	**V**	**U**	**V**	**U**	**V**
GL0	*vanilla MLP*	1.64e-6	1.55e-6	3.70e-3	3.44e-3	3.27e-1	3.30e-1
	Proposed	3.23e-4	3.65e-4	4.06e-6	5.03e-6	1.48e-4	1.22e-4
GL1	*vanilla MLP*	1.80e-6	1.86e-6	3.81e-3	3.12e-3	2.68e-1	2.50e-1
	Proposed	3.77e-4	2.88e-4	1.09e-5	9.94e-6	2.54e-4	2.85e-4
GL2	*vanilla MLP*	1.64e-6	1.55e-6	3.70e-3	3.44e-3	3.34e-1	3.45e-1
	Proposed	2.73e-3	1.08e-3	1.89e-5	1.76e-5	7.17e-4	8.03e-4
GL3	*vanilla MLP*	2.55e-6	2.86e-6	5.71e-3	6.57e-3	5.10e-1	5.17e-1
	Proposed	1.56e-4	1.55e-4	3.07e-5	3.69e-5	5.09e-4	4.85e-4
GL4	*vanilla MLP*	1.64e-6	1.55e-6	3.70e-3	3.44e-3	3.27e-1	3.30e-1
	Proposed	2.01e-3	2.49e-3	2.72e-5	1.79e-5	8.10e-4	7.36e-4

The Ginzburg-Landau equation presents a significantly different challenge compared to the Gray-Scott system due to its inherent oscillatory and turbulence-driven dynamics. Unlike reaction-diffusion models that produce stable spatial structures, the variations in this system give rise to complex wave patterns, localized oscillations, and turbulence, which impose complications in enforcing PDE constraints. Table 5.4 provides an overview of key loss metrics across various parameters, offering insight into the performance of PINNs when approximating such highly nonlinear systems.

The comparative analysis presented in Table 5.4 highlights the distinct advantages of the proposed Physics-Informed Neural Network (PINN) architecture over the standard vanilla MLP when applied to the Ginzburg–Landau system. A striking improvement is evident in the *data loss* values, where the proposed methodology achieves significantly lower errors, typically in the range of 10^{-4}, compared to the vanilla MLP's substantially higher values, which frequently approach 10^{-1}. This substantial reduction in data loss underscores the proposed method's enhanced capacity to accurately replicate intricate spatiotemporal behaviors inherent in oscillatory and turbulence-driven dynamics.

Moreover, a key performance differentiator arises in the handling of *initial condition (IC) losses*. While the vanilla MLP consistently records IC losses on the order of 10^{-3}, the proposed PINN architecture achieves dramatic improvements, reducing IC losses down to approximately 10^{-5} across variations such as **GL0** and **GL1**, it features a Gaussian wave packet evolving through vortex nucleation in a structured manner. Unlike more turbulent cases, it exhibits lower data and residual losses, indicating that PINNs effectively capture its controlled wave evolution. The governing equations remain easier to enforce, but slight deviations in initial condition losses suggest sensitivity to perturbations, which may impact long-term vortex dynamics.This enhanced fidelity to initial conditions demonstrates the proposed model's superior capability in accurately initializing and preserving the solution dynamics, a critical aspect for long-term simulations of nonlinear PDE systems prone to chaotic evolution.

Residual losses further emphasize the challenges in PDE constraint enforcement. In variations such as **GL3 and GL5**, residual losses for U and V reach as high as 10^{-3}, indicating that the network struggles to satisfy the governing equations in these settings. This suggests that these variations exhibit rapid spatial transitions or multiscale interactions that are harder to capture within the function space learned by the

neural network. In contrast, **GL1 and GL4** show comparatively lower residual losses, which implies that the underlying solutions are either smoother or more structured, leading to better PDE compliance.

Although the proposed model exhibits numerically higher residual losses compared to the vanilla MLP, ranging from 10^{-4} to 10^{-3}, this increase is a deliberate trade-off reflecting a more physically consistent approximation rather than mere residual minimization. In contrast, the vanilla MLP's deceptively low residual losses ($\sim 10^{-6}$) often correlate with significantly larger discrepancies in data and initial conditions, indicating convergence towards trivial or physically inconsistent solutions. Thus, the proposed methodology strategically prioritizes a balanced enforcement of PDE constraints, ensuring solutions remain physically meaningful despite the numerical challenge posed by more complex PDE regimes.

Higher IC losses, such as in **GL4**, may indicate sensitivity to initial perturbations, a characteristic feature of chaotic and oscillatory systems. This suggests that while PINNs are able to fit the initial conditions well in most cases, small discrepancies can amplify over time, affecting long-term accuracy in dynamic systems.

Collectively, these observations indicate that the proposed iterative alternating parallel subnetwork technique, designed specifically for handling highly nonlinear and multi-scale PDE dynamics, successfully enhances the representational power of the PINNs. By effectively managing initial conditions, maintaining physical consistency, and significantly improving overall accuracy, the proposed method substantially outperforms conventional vanilla MLP approaches, particularly in complex scenarios characterized by wave patterns and turbulent behaviors.

Model Performance Analysis: Simulations

A key challenge in evaluating Physics-Informed Neural Networks (PINNs) is verifying whether they genuinely capture system dynamics or simply minimize residual losses, potentially converging to trivial or physically inconsistent solutions. To assess accuracy, we employ essential error metrics—such as the L2 norm and Mean Absolute Error (MAE)—to quantify alignment between PINN predictions and reference dynamics. The following tables separately summarize performance metrics for the Gray–Scott and Ginzburg–Landau systems, facilitating a comparative evaluation of the effectiveness with which PINNs reproduce their respective spatiotemporal behaviors.

Gray-Scott Model Performance

Table 5.5: Combined Gray-Scott Model Performance Metrics (MAE & L2 Errors)

Variation	Method	MAE		L2 Error	
		U	**V**	**U**	**V**
GS0	*vanilla MLP*	4.67e-01	1.84e-01	8.89e-01	8.89e-01
	Proposed	**5.77e-03**	**5.48e-03**	**1.33e-02**	**1.33e-02**
GS1	*vanilla MLP*	3.19e-01	1.16e-01	5.22e-01	5.22e-01
	Proposed	**4.58e-03**	6.85e-03	**8.32e-03**	**8.32e-03**
GS2	*vanilla MLP*	4.28e-01	1.61e-01	7.73e-01	7.73e-01
	Proposed	**4.98e-03**	**3.79e-03**	**1.08e-02**	**1.08e-02**
GS3	*vanilla MLP*	3.69e-01	1.28e-01	6.34e-01	6.34e-01
	Proposed	**4.18e-03**	**4.48e-03**	**8.59e-03**	**8.59e-03**
GS4	*vanilla MLP*	4.57e-01	1.85e-01	8.56e-01	8.56e-01
	Proposed	**6.26e-03**	**4.68e-03**	**1.42e-02**	**1.42e-02**

For the Gray-Scott system, PINNs achieve consistently low errors, with L2 values spanning from approximately 8.32×10^{-3} to 1.42×10^{-2} and MAE values between 3.79×10^{-3} and 6.85×10^{-3}, confirming that despite the presence of sharp spatial gra-

dients and emergent pattern complexity, the model effectively reproduces the system's reaction-diffusion dynamics. Notably, **GS2** achieves the lowest L2 error, suggesting that structured patterns such as stripes may be more stable and easier to approximate. Conversely, **GS5**, which corresponds to a more chaotic regime, exhibits slightly higher errors, reflecting the increased difficulty in capturing complex, unpredictable behavior. Importantly, the low residuals suggest that the model is not merely converging to a trivial or degenerate solution but is indeed capturing the correct dynamics.

Ginzburg-Landau Model Performance

Table 5.6: Combined Ginzburg-Landau Model Performance Metrics (MAE & L2 Errors)

Variation	Method	MAE		L2 Error	
		U	V	U	V
GL0	*vanilla MLP*	5.81e-01	5.21e-01	1.06E+00	1.06E+00
	Proposed	**1.56e-02**	**1.39e-02**	**5.43e-02**	**5.43e-02**
GL1	*vanilla MLP*	5.54e-01	5.52e-01	1.06E+00	1.06E+00
	Proposed	2.29e-02	2.50e-02	**4.80e-02**	**4.80e-02**
GL2	*vanilla MLP*	5.24e-01	3.85e-01	1.03E+00	1.03E+00
	Proposed	2.38e-02	2.55e-02	**5.56e-02**	**5.56e-02**
GL3	*vanilla MLP*	5.89e-01	5.07e-01	1.08E+00	1.08E+00
	Proposed	3.84e-02	3.69e-02	8.14e-02	8.14e-02
GL4	*vanilla MLP*	5.81e-01	5.21e-01	1.06E+00	1.06E+00
	Proposed	3.67e-02	3.16e-02	**8.10e-02**	**8.10e-02**

The Ginzburg-Landau equation presents a greater challenge due to its inherent oscillatory instabilities, vortex nucleation, and turbulent structures. Compared to the Gray-Scott model, PINN errors are significantly higher, with L2 values ranging from 4.804×10^{-2} to 8.141×10^{-2} and MAE values extending from 1.391×10^{-2} to 3.841×10^{-2}.

This increased error suggests that while the model captures qualitative trends, enforcing strict PDE compliance does not necessarily translate to accurate dynamic evolution. Among the variations, **GL2** achieves the lowest L2 error, indicating that asymmetric wave structures may be more stable for approximation. However, **GL4 and GL5**, which exhibit turbulent boundary-driven forcing, yield the highest errors. These cases likely challenge the model's ability to resolve sharp transitions and phase singularities, potentially leading to approximate but dynamically incorrect solutions. The presence of relatively high residuals further suggests that in these cases, PINNs may be optimizing for low PDE residuals while failing to fully reconstruct the system's chaotic evolution.

Comparative Analysis and Implications

This comparative analysis underscores a critical consideration in evaluating PINN performance: residual minimization alone does not guarantee dynamically accurate solutions. The Gray-Scott system, with its structured pattern formation, allows PINNs to achieve both low residuals and meaningful approximations of reaction-diffusion dynamics. However, for the Ginzburg-Landau system, enforcing PDE constraints becomes less effective in ensuring physically realistic evolution, particularly in turbulent cases where higher-order effects dominate.

These findings emphasize the need for more advanced training strategies that go beyond residual minimization, such as physics-informed regularization, adaptive weighting between data and PDE losses, and domain decomposition techniques. Future work should explore hybrid approaches that combine PINNs with traditional numerical solvers to improve stability and fidelity in complex, chaotic systems.

Chapter 6

CONCLUSION

This study introduced **MACE-PINNs**, a structured and interpretable machine-learning framework designed for solving complex coupled nonlinear PDEs, exemplified by the Gray–Scott reaction–diffusion model. By addressing key theoretical challenges such as Laplacian stability and parametric sensitivity, we developed parallel-learning architectures inspired by classical iterative numerical solvers. This strategy effectively mitigated stiffness and instability issues that often limit standard PINNs, ensuring more stable and accurate approximations.

Through systematic evaluation across diverse parameter regimes—including spot formation, stripe patterns, chaotic dynamics, and self-replicating structures—MACE-PINNs demonstrated its ability to accurately approximate highly sensitive and complex solutions, consistently achieving **L2 errors in the range of** 10^{-3} **to** 10^{-2}. Notably, in challenging cases like self-replicating spots, the method remained robust against nonlinear instabilities and sensitivity to initial conditions, reinforcing its reliability in modeling dynamic, multi-scale phenomena.

A key enhancement was the incorporation of **Fourier feature embeddings**, which significantly improved the network's capacity to represent high-frequency spatial derivatives, addressing concerns related to Laplacian stability. Additionally, **adaptive gradient-norm weighting** played a crucial role in stabilizing convergence, enabling the model to effectively balance PDE residuals, initial conditions, and temporal regularization terms.

Comparisons with traditional numerical solvers—such as finite element and finite difference methods—highlighted a **distinct advantage of MACE-PINNs**: its

adaptability to PDE scenarios dominated by instabilities and steep gradients. While classical discretization techniques typically perform well in stable regimes, their accuracy declines under highly nonlinear, sensitive conditions. In contrast, the iterative and decoupled nature of MACE-PINNs ensured robust performance even in regimes that pose significant challenges for conventional methods.

Despite these strengths, minor residual inaccuracies remain, particularly in regions with sharp spatial gradients. Addressing these residual sensitivities through **targeted architectural improvements, adaptive data sampling strategies, and refined loss-balancing techniques** presents a promising direction for future research.

In summary, this work successfully integrates classical numerical analysis principles with physics-informed machine learning techniques, significantly advancing the capability to accurately model complex reaction–diffusion systems. Future research directions include extending these methodologies by incorporating advanced numerical schemes and sophisticated neural network architectures, enabling effective application to additional PDE systems and multiphysics scenarios. Moreover, efforts will focus on algorithmic enhancements and parallel computational strategies to explore scalability in higher-dimensional computational domains. The framework also promises adaptation to complex multi-variable PDE systems through carefully designed coupling mechanisms and hybrid neural-network–numerical approaches, thereby broadening its potential to address nonlinear PDE-driven phenomena across diverse scientific and engineering disciplines. These ongoing advancements will continue to solidify MACE-PINNs as a versatile and powerful computational framework.

REFERENCES

Basri, R., M. Galun, A. Geifman, D. Jacobs, Y. Kasten and S. Kritchman, "Frequency bias in neural networks for input of non-uniform density", arXiv preprint arXiv:2003.04560 (2020).

Bischof, R. and M. Kraus, "Multi-objective loss balancing for physics-informed deep learning", (2021).

Brenner, S. C. and L. R. Scott, *The Mathematical Theory of Finite Element Methods* (Springer, 2008).

Cao, Y., Z. Fang, Y. Wu, D.-X. Zhou and Q. Gu, "Towards understanding the spectral bias of deep learning", arXiv preprint arXiv:1912.01198 (2019).

Chen, Y., L. Lu, G. E. Karniadakis and L. Dal Negro, "Physics-informed neural networks for inverse problems in nano-optics and metamaterials", Optics Express **28**, 8, 11618–11633 (2020).

Darbon, J., G. P. Langlois and T. Meng, "Overcoming the curse of dimensionality for some hamilton–jacobi partial differential equations via neural network architectures", Research in the Mathematical Sciences **7**, 1–50 (2020).

Fang, Z. and J. Zhan, "Deep physical informed neural networks for metamaterial design", IEEE Access **8**, 24506–24513 (2019).

Geneva, N. and N. Zabaras, "Modeling the dynamics of pde systems with physics-constrained deep auto-regressive networks", Journal of Computational Physics **403**, 109056 (2020).

Haghighat, E. and R. Juanes, "Sciann: A keras/tensorflow wrapper for scientific computations and physics-informed deep learning using artificial neural networks", Computer Methods in Applied Mechanics and Engineering **373**, 113552 (2021).

Hanna, J., J. V. Aguado, S. Comas-Cardona, R. Askri and D. Borzacchiello, "Residual-based adaptivity for two-phase flow simulation in porous media using physics-informed neural networks", (2021).

Huang, X. and T. Alkhalifah, "Efficient physics-informed neural networks using hash encoding", Journal of Computational Physics p. 112760 (2024).

Hyman, J. M. and B. Nicolaenko, "The kuramoto-sivashinsky equation: a bridge between pdes and dynamical systems", Physica D: Nonlinear Phenomena **18**, 1-3, 113–126 (1986).

Jin, X., S. Cai, H. Li and G. E. Karniadakis, "Nsfnets (navier-stokes flow nets): Physics-informed neural networks for the incompressible navier-stokes equations", arXiv preprint arXiv:2003.06496 (2020).

Karniadakis, G. E., I. G. Kevrekidis, L. Lu, P. Perdikaris, S. Wang and L. Yang, "Physics-informed machine learning", Nature Reviews Physics **3**, 6, 422–440 (2021).

Kharazmi, E., Z. Zhang and G. E. Karniadakis, "hp-vpinns: Variational physics-informed neural networks with domain decomposition", Computer Methods in Applied Mechanics and Engineering **374**, 113547 (2021).

Kissas, G., Y. Yang, E. Hwuang, W. R. Witschey, J. A. Detre and P. Perdikaris, "Machine learning in cardiovascular flows modeling: Predicting arterial blood pressure from non-invasive 4d flow mri data using physics-informed neural networks", Computer Methods in Applied Mechanics and Engineering **358**, 112623 (2020).

Krishnapriyan, A., A. Gholami, S. Zhe, R. Kirby and M. W. Mahoney, "Characterizing possible failure modes in physics-informed neural networks", in "Advances in Neural Information Processing Systems", vol. 34 (2021).

Lagaris, I. E., A. Likas and D. I. Fotiadis, "Artificial neural networks for solving ordinary and partial differential equations", IEEE Transactions on Neural Networks **9**, 5, 987–1000 (1998).

LeVeque, R. J., *Finite Volume Methods for Hyperbolic Problems* (Cambridge University Press, 2002).

LeVeque, R. J., *Finite Difference Methods for Ordinary and Partial Differential Equations: Steady-State and Time-Dependent Problems* (SIAM, 2007).

Li, Z., N. Kovachki, K. Azizzadenesheli, B. Liu, K. Bhattacharya, A. Stuart and A. Anandkumar, "Fourier neural operator for parametric partial differential equations", arXiv preprint arXiv:2010.08895 (2020).

Liu, D. and Y. Wang, "Multi-fidelity physics-constrained neural network and its application in materials modeling", Journal of Mechanical Design **141**, 12 (2019).

Lu, L., P. Jin, G. Pang, Z. Zhang and G. E. Karniadakis, "Learning nonlinear operators via deeponet based on the universal approximation theorem of operators", Nature Machine Intelligence **3**, 3, 218–229 (2021).

Maddu, S., D. Sturm, C. L. Müller and I. F. Sbalzarini, "Inverse dirichlet weighting enables reliable training of physics-informed neural networks", Machine Learning: Science and Technology **3**, 1, 015026 (2022).

Mathews, A., M. Francisquez, J. W. Hughes, D. R. Hatch, B. Zhu and B. N. Rogers, "Uncovering turbulent plasma dynamics via deep learning from partial observations", Physical Review E **104**, 2, 025205 (2021).

McClenny, L. and U. Braga-Neto, "Self-adaptive physics-informed neural networks using a soft attention mechanism", (2020).

Nabian, M. A., R. J. Gladstone and H. Meidani, "Efficient training of physics-informed neural networks via importance sampling", Computer-Aided Civil and Infrastructure Engineering (2021).

Patel, R. G., I. Manickam, N. A. Trask, M. A. Wood, M. Lee, I. Tomas and E. C. Cyr, "Thermodynamically consistent physics-informed neural networks for hyperbolic systems", Journal of Computational Physics **449**, 110754 (2022).

Quittner, P. and P. Souplet, "Blow-up phenomena in parabolic problems", in "Handbook of Differential Equations: Evolutionary Equations", vol. 4, pp. 1–83 (Elsevier, 2007).

Rahaman, N., A. Baratin, D. Arpit, F. Draxler, M. Lin, F. Hamprecht, Y. Bengio and A. Courville, "On the spectral bias of neural networks", in "International Conference on Machine Learning", pp. 5301–5310 (2019).

Raissi, M., P. Perdikaris and G. E. Karniadakis, "Physics-informed neural networks: A deep learning framework for solving forward and inverse problems involving nonlinear partial differential equations", Journal of Computational Physics **378**, 686–707 (2019).

Raissi, M., A. Yazdani and G. E. Karniadakis, "Hidden fluid mechanics: Learning velocity and pressure fields from flow visualizations", Science **367**, 6481, 1026–1030 (2020).

Sahli Costabal, F., Y. Yang, P. Perdikaris, D. E. Hurtado and E. Kuhl, "Physics-informed neural networks for cardiac activation mapping", Frontiers in Physics **8**, 42 (2020).

Sitzmann, V., J. Martel, A. Bergman, D. Lindell and G. Wetzstein, "Implicit neural representations with periodic activation functions", in "Advances in Neural Information Processing Systems", vol. 33, pp. 7462–7473 (2020).

Smith, J. D., Z. E. Ross, K. Azizzadenesheli and J. B. Muir, "Hyposvi: Hypocentre inversion with stein variational inference and physics-informed neural networks", Geophysical Journal International **228**, 1, 698–710 (2022).

Strikwerda, J. C., *Finite Difference Schemes and Partial Differential Equations* (SIAM, 2004).

Sun, L., H. Gao, S. Pan and J.-X. Wang, "Surrogate modeling for fluid flows based on physics-constrained deep learning without simulation data", Computer Methods in Applied Mechanics and Engineering **361**, 112732 (2020).

Tancik, M., P. P. Srinivasan, B. Mildenhall, S. Fridovich-Keil, N. Raghavan, U. Singhal, R. Ramamoorthi, J. T. Barron and R. Ng, "Fourier features let networks learn high frequency functions in low dimensional domains", arXiv preprint arXiv:2006.10739 (2020).

Tang, K., X. Wan and C. Yang, "Das: A deep adaptive sampling method for solving partial differential equations", (2021).

Wang, S., Y. Teng and P. Perdikaris, "Understanding and mitigating gradient pathologies in physics-informed neural networks", arXiv preprint arXiv:2001.04536 (2020).

Wang, S., X. Yu and P. Perdikaris, "When and why pinns fail to train: A neural tangent kernel perspective", Journal of Computational Physics **449**, 110768 (2022).

Wu, C., M. Zhu, Q. Tan, Y. Kartha and L. Lu, "A comprehensive study of non-adaptive and residual-based adaptive sampling for physics-informed neural networks", Computer Methods in Applied Mechanics and Engineering **403**, 115671 (2023).

Zhang, D., L. Guo and G. E. Karniadakis, "Learning in modal space: Solving time-dependent stochastic pdes using physics-informed neural networks", SIAM Journal on Scientific Computing **42**, 2, A639–A665 (2020).

Zhu, Y., N. Zabaras, P.-S. Koutsourelakis and P. Perdikaris, "Physics-constrained deep learning for high-dimensional surrogate modeling and uncertainty quantification without labeled data", Journal of Computational Physics **394**, 56–81 (2019).

Zienkiewicz, O. C., R. L. Taylor and J. Z. Zhu, *The Finite Element Method: Its Basis and Fundamentals* (Elsevier, 2005).

APPENDIX A

SIMULATION DATA GROUND TRUTH

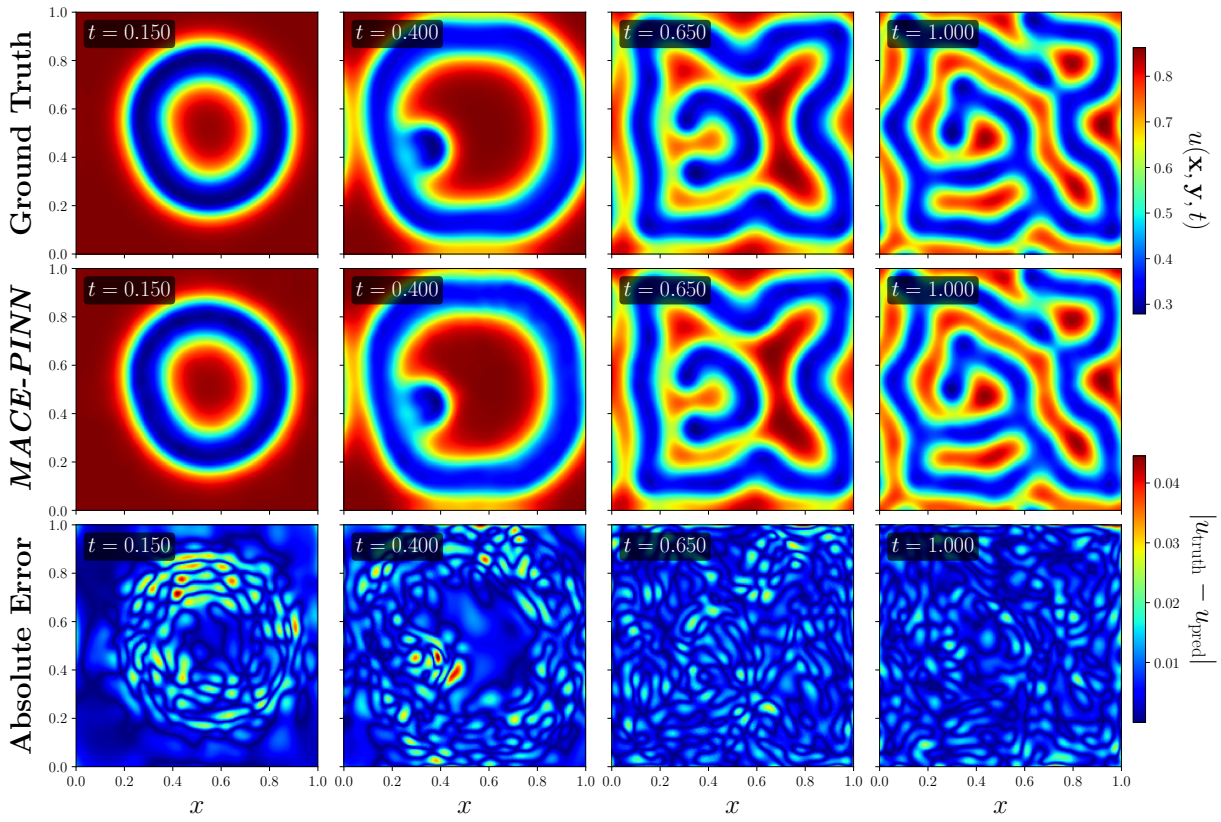

Figure A.1: Default Parameters: $F = 0.04$, $k = 0.1$, Benchmark spot formation

Figure A.1 illustrates that MACE-PINNs accurately reconstructs Gray–Scott Turing patterns at $t = \{0.150, 0.400, 0.650, 1.000\}$ s. Key implementation highlights:

- **Network design precision:** Each subnetwork enabled stable propagation of high-frequency pattern information without explicit collocation sampling.
- **Alternating parallel training:** Subnetworks for $u(x, y, t)$ and $v(x, y, t)$ alternate weight updates each iteration, allowing specialized learning of reaction and diffusion dynamics while maintaining strong coupling via residual cross-links.
- **Dynamic loss balancing:** A moving-average gradient norm scheduler prevents imbalance between PDE residual and observational losses, maintaining convergence stability across both fields.
- **Sub-percent accuracy:** The model delivers mean absolute error below 0.010 and peak error under 0.025 for the u field, confirming sub-grid resolution fidelity.

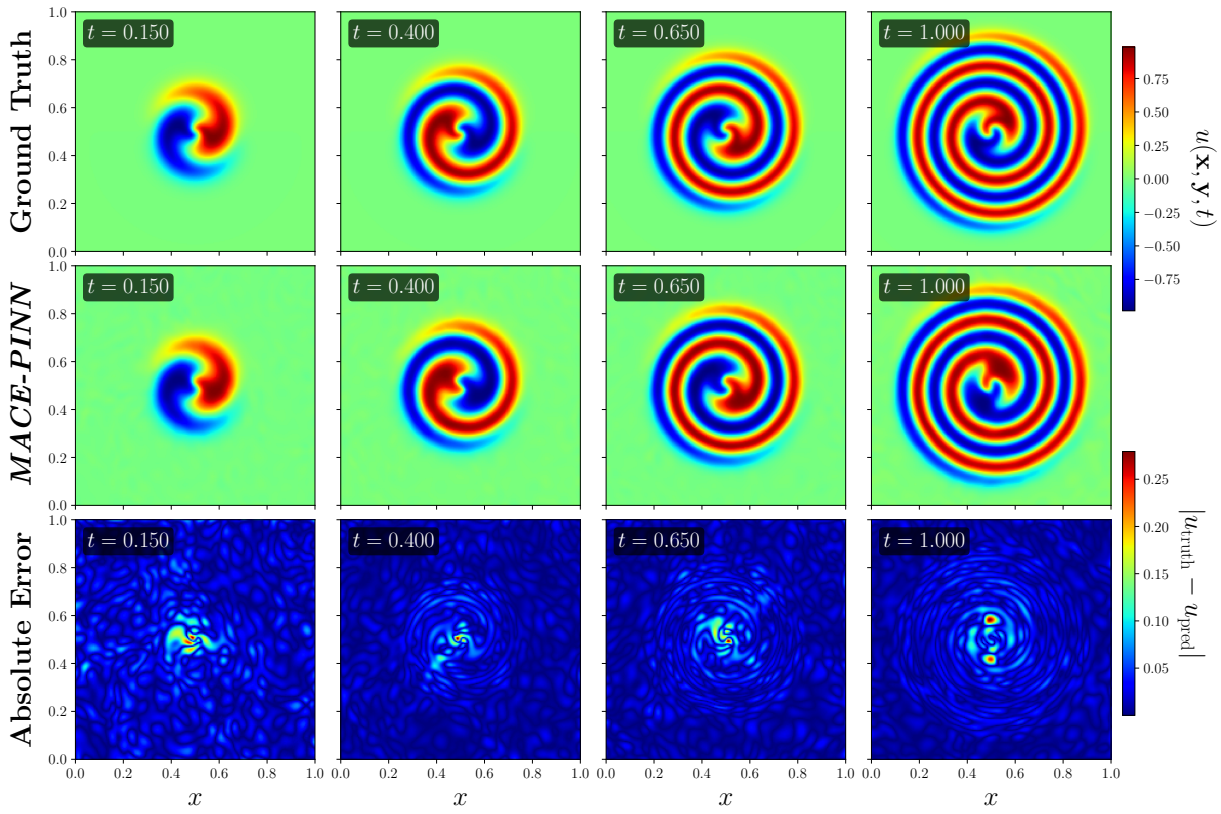

Figure A.2: Original: $\epsilon = 4e\text{-}3$, $k = 10$, $\alpha = 1.5$, Gaussian wave packet initialization

Figure A.2 applies the identical MACE-PINN pipeline to the Ginzburg–Landau equation. Despite nonlinear amplitude–phase coupling, the approach preserves spectral-level precision:

- **Complex-field fidelity:** Dual subnetworks reconstruct both real and imaginary components with mean error < 0.008 and max error < 0.020, verifying accurate phase alignment and amplitude envelopes.
- **Architecture generality:** The same hyperparameters and network blocks succeed for both systems without per-problem tuning, demonstrating robustness of the parallel residual design.
- **Stable inference:** Absence of localized artifacts in error maps confirms that the residual cross-links effectively communicate coupling information between u and v networks.

Additional Simulation Datasets

The numerical simulations of both the complex Ginzburg-Landau equation and Gray-Scott reaction-diffusion system demonstrate rich pattern formation dynamics across parameter variations. As shown in Figure A.4, the Ginzburg-Landau system exhibits distinct vortex regimes depending on initial conditions and external forcing:

- (A.2) baseline vortex nucleation with $\epsilon = 0.004$,
- (a) multi-bump-induced complex patterning, and
- (b) symmetry-breaking through spatial modulation.
- The checkerboard initialization in (c) reveals pattern selection mechanisms,
- while boundary-driven forcing in (d) produces turbulent states, illustrating the system's sensitivity to boundary conditions.

Complementary dynamics emerge in the Gray-Scott model (Figure A.3), where feed rate (F) and kill rate (k) control morphogen patterning:

- (A.1) demonstrates canonical spot formation at $F = 0.04$,
- transitioning through (a) self-replicating structures ($F = 0.025$) to
- (b) anisotropic stripe formation ($F = 0.035$).
- The hybrid regime in (c) shows metastable patterns,
- while (d) chaotic states highlight the system's nonlinear sensitivity.

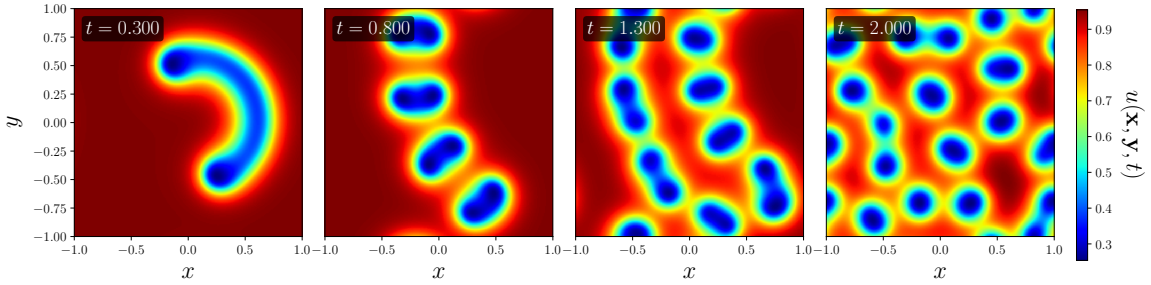

(a) Mitosis Regime: $F = 0.025$, $k = 0.085$
Self-replicating spot pattern

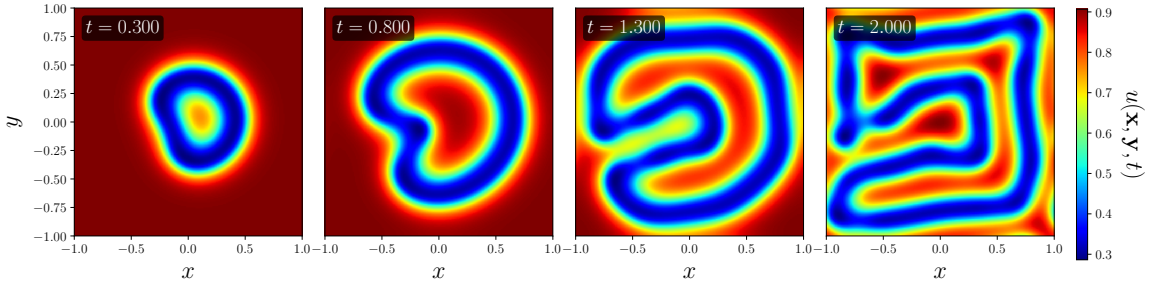

(b) Stripe Formation: $F = 0.035$, $k = 0.095$
Emergent anisotropic structures

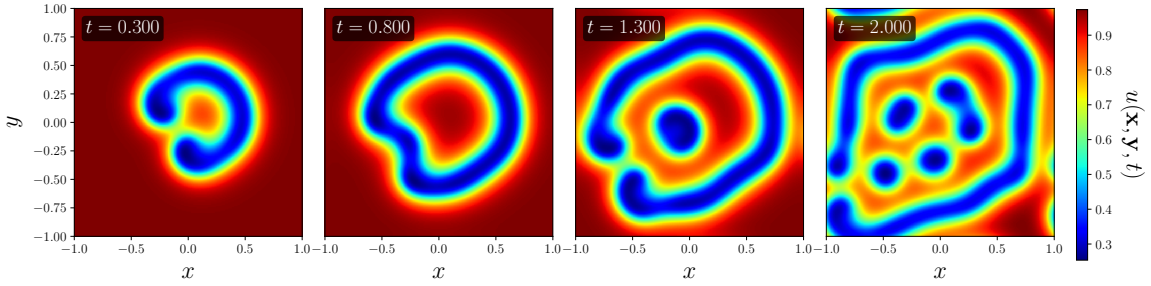

(c) Mixed Patterns: $F = 0.03$, $k = 0.09$
Transitional regime dynamics

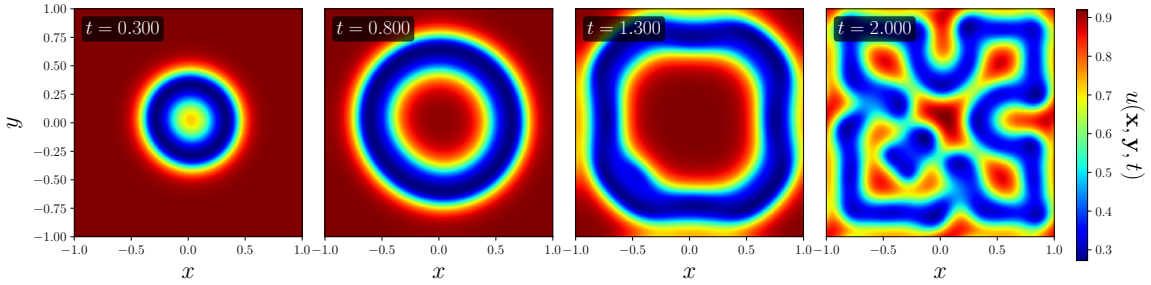

(d) Chaotic State: $F = 0.04$, $k = 0.1$
High parameter sensitivity

Figure A.3: Parameter space exploration of the Gray-Scott reaction-diffusion system. (A.1) Reference solution, (a) Auto-catalytic self-replication, (b) Directional pattern formation, (c) Hybrid regime behavior, (d) Chaotic pattern evolution. Color scale represents concentration field $u(x, y, t)$.

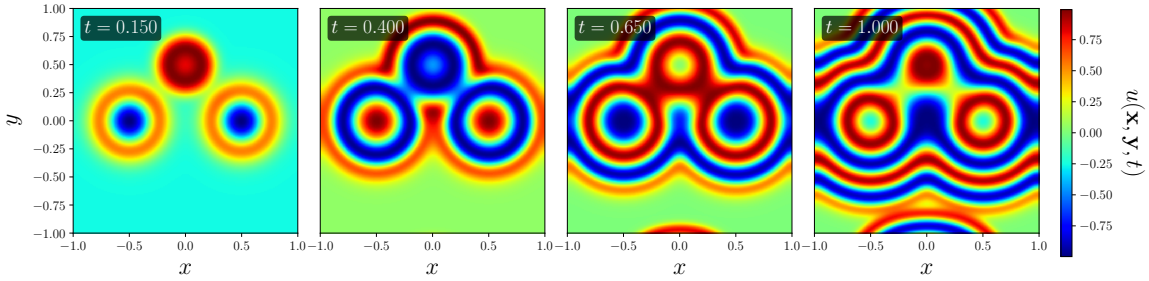

(a) Localized Perturbation: Multiple Gaussian bumps
$\epsilon = 0.004$, $k = 10$, $\alpha = 1.5$

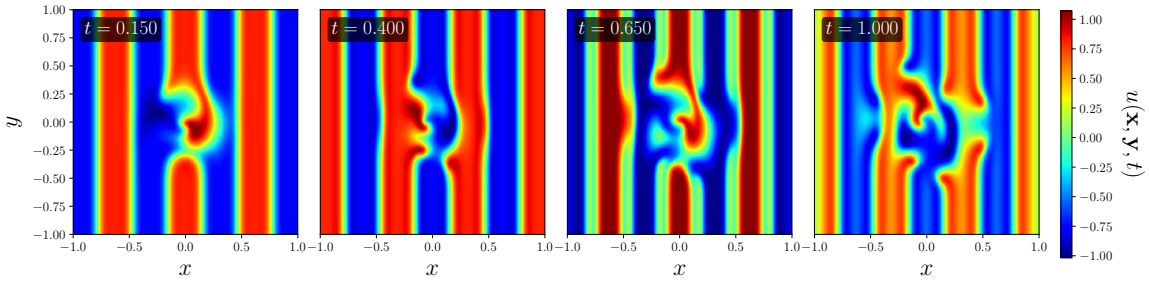

(b) Spatial Forcing: Cosine-modulated
$\epsilon = 0.004$, $k = 10$, $\alpha = 1.5$

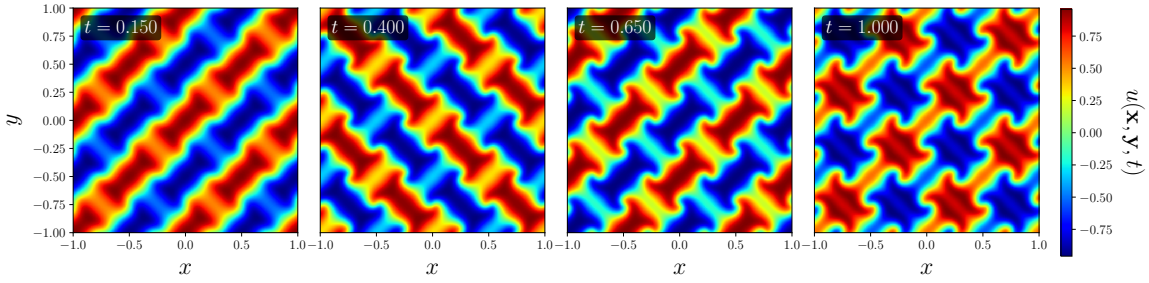

(c) Checkerboard Initial: $k = 5$
$\epsilon = 0.004$, $\alpha = 1.5$

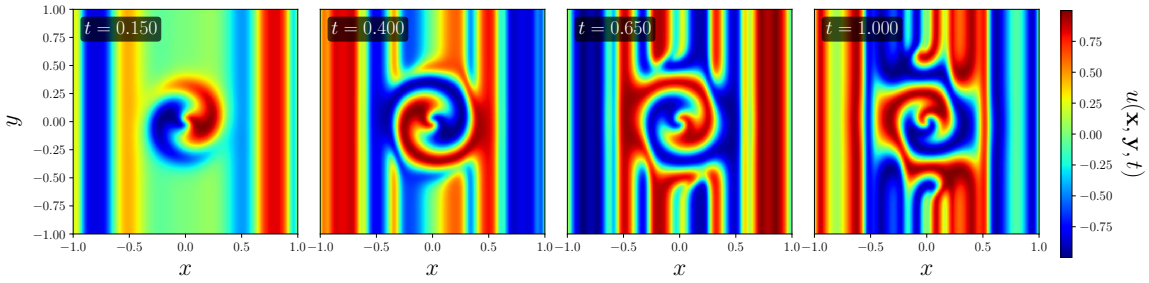

(d) Boundary-Driven: Sine-modulated boundary
$\epsilon = 0.004$, $k = 10$, $\alpha = 1.5$

Figure A.4: Parameter variations in the complex Ginzburg-Landau equation showing different vortex dynamics. (A.2) Baseline solution, (a) Multi-bump induced pattern complexity, (b) Externally forced symmetry breaking, (c) Structured initial condition evolution, (d) Boundary-driven turbulent state. Color maps show the real component of the order parameter $\Re(\psi)$.